Sensors and Actuators A 244 (2016) 95–105

Contents lists available at ScienceDirect

Sensors and Actuators A: Physical

journal homepage: www.elsevier.com/locate/sna

Odd-harmonic repetitive control for high-speed raster scanning of piezo-actuated nanopositioning stages with hysteresis nonlinearity

Chun-Xia Li [a], Guo-Ying Gu [a], Li-Min Zhu [a,*], Chun-Yi Su [b]

[a] State Key Laboratory of Mechanical System and Vibration, School of Mechanical Engineering, Shanghai Jiao Tong University, Shanghai 200240, China
[b] Department of Mechanical and Industrial Engineering, Concordia University, Montreal, QC H3G 1M8, Canada

ARTICLE INFO

Article history:
Received 15 January 2016
Received in revised form 18 March 2016
Accepted 4 April 2016
Available online 11 April 2016

Keywords:
Piezoelectric actuator
Nanopositioning stage
Odd-harmonic repetitive control
Hysteresis compensation
Raster scanning

ABSTRACT

In raster scanning applications of atomic force microscopies, precisely tracking periodic triangular trajectories is the major objective of nanopositioning stages. Considering the fact of periodic operations, the repetitive control technique becomes promising and has been recently developed to reduce tracking errors. In our new experiments, it is found that, with triangular reference input, the hysteresis nonlinearity mainly affects the system at the odd harmonics of the input signal. In this sense, an odd-harmonic repetitive control (ORC) strategy is proposed to handle the hysteresis nonlinearity, with the hysteresis treated as the odd-harmonic periodic disturbance. Therefore, it avoids the modeling and inverting of the complex hysteresis nonlinearity. Another benefit of the developed ORC strategy is that it can also account for the tracking errors caused by the linear dynamics effect. To verify the effectiveness of the ORC strategy, real-time experiments are performed on a custom-built piezo-actuated nanopositioning stage. Experimental results show that the developed ORC strategy achieves precise tracking of 1562.5-Hz triangular trajectory with the hysteresis nonlinearity mitigated to a negligible level, which demonstrates the feasibility and effectiveness of the developed ORC strategy on hysteresis compensation during high-speed raster scanning.

1. Introduction

With the ability of imaging sample surface with nanometer/sub-nanometer resolution, atomic force microscopies (AFMs) have been playing an important role in many applications [1]. A key component of the AFM is a nanopositioner which is usually driven in a raster pattern along the lateral direction, so as to scan the probe relative to the sample surface for imaging. Piezoelectric tube scanners (PTSs) are the most commonly utilized nanopositioners in early AFMs [2]. Recently, besides high-precision scanning, high-speed operation of AFMs is increasingly demanded, for instance, in the application of imaging sample with a fast time-varying nature [3,4]. Due to the advantage of larger mechanical bandwidth, the flexure-based nanopositioning stages are gradually overtaking the PTSs as the nanopositioners of high-speed AFMs [2].

Most flexure-based nanopositioning stages utilize piezoelectric stack actuators (PSAs) for actuation due to their merits of ultra-high resolution and fast response [5]. However, the nanopositioning stages suffer from the hysteresis nonlinearity of the PSAs and the dynamics effect of the flexure-based mechanism, which severely degrade its tracking performance [6]. To deal with the hysteresis nonlinearity, various control strategies have been proposed, such as charge control [7], inversion-based feedforward control [8–10], and robust feedback control [11–13]. In addition, other control approaches with specific characteristics, like the phase control [14,15], have also been developed to reduce the hysteresis nonlinearity. For a comprehensive study of the control methods to account for the hysteresis nonlinearity, readers can refer to [6] and references therein. It should be noted that the recent reports have revealed that the hysteresis nonlinearity becomes more evident and serious with the increase of input frequencies [16,17]. In addition, during high-speed tracking, the hysteresis nonlinearity and the dynamics effect of the nanopositioning stage are usually coupled to affect the tracking performance [18], which may cause tracking errors beyond 35% [6]. Such coupling effect makes it more challenging to develop effective controller for high-speed raster scanning of the nanopositioning stages.

In raster scanning applications of AFMs, precisely tracking periodic triangular trajectories is the major objective of nanopositioning stages [18]. Considering the fact of such periodic operation, the repetitive control (RC) technique becomes attractive. For the conventional repetitive control (CRC), a signal generator $1/(z^N - 1)$

* Corresponding author.
E-mail address: zhulm@sjtu.edu.cn (L.-M. Zhu).

http://dx.doi.org/10.1016/j.sna.2016.04.009
0924-4247/

(N is the sampling number in each fundamental period of the reference) is included into the feedback loop to provide high-gain control at the harmonics of the reference trajectory. Such high gains make the CRC capable of precisely tracking periodic trajectory. Hence, CRC is promising for the raster scanning of AFMs and has been recently investigated to reduce the tracking errors of nanopositioning stages in such applications. However, the generally utilized CRC is a control scheme for linear systems and the hysteresis nonlinearity of the PSAs restricts its direct application to the nanopositioning stages. To deal with the hysteresis nonlinearity, a commonly used approach is the integration of an inverse hysteresis compensator (IHC) with the CRC. For example, in [19,20], the CRC strategy is applied to nanopositioning stages in combination with an IHC in the feedforward path. In these works, a main task is the construction of an IHC. However, it is generally time-consuming and complicated to construct an accurate hysteresis model and its inversion [11], especially in the case of high-speed tracking where the hysteresis nonlinearity and dynamics effect are coupled [18]. The IHC also increases the complexity of the controller design and implementation. Furthermore, the inverse hysteresis compensation error always exists and it is not easy and sometimes impossible to derive its analytical expression, which thus makes the stability analysis of the system with IHC difficult [6]. Alternatively, in [21,22], the hysteresis is considered to be suppressed by the existing feedback controller and then the CRC is implemented. However, the tracking frequencies in these applications are generally low, where the hysteresis nonlinearity is not so serious and complex as that of high frequencies.

In our previous work [23], it has been theoretically analyzed that the hysteresis nonlinearity of PSAs with periodic reference input can be decomposed as a periodic disturbance over a linear system. As a further investigation, in our new experiments, it is found that with the triangular reference input the hysteresis nonlinearity mainly affects the system at the odd harmonics of the input signal. In this sense, an odd-harmonic repetitive control (ORC) strategy is proposed to handle the hysteresis nonlinearity by treating it as the odd-harmonic disturbance. Therefore, the modeling and inverting of complex hysteresis nonlinearity are avoided. Another benefit of the ORC is that it can also account for the tracking errors caused by the linear dynamics effect as they are also odd-harmonic signals under triangular trajectory. It is worthy of mentioning that, as the ORC strategy employs a different signal generator in the form of $(-1/(z^{N/2}+1))$ to provide high-gain control only at the odd harmonics of the reference trajectory, the ORC reduces the data memory occupation by 50% as compared to CRC, which is beneficial for real-time implementation. This is why the ORC rather than the CRC is adopted in this work to achieve high-speed raster scanning of the piezo-actuated nanopositioning stages with hysteresis nonlinearity. It should be noted that although ORC strategy has been successfully applied to power electronics systems for tracking odd-harmonic periodic references [24,25], the application of ORC to nanopositioning stages with complicated hysteresis nonlinearity is still limited. In the literature, only Shan and Leang [26] have reported a type of ORC for the tracking control of nanopositioning stages. However, in their work, the hysteresis nonlinearity is mitigated with an IHC and the ORC is cascaded with a CRC as a dual-RC application to further improve the positioning performance, which may be complicated and thus leads to insufficient memory of the hardware for real-time implementation [26]. Therefore, from the literature, it is still a new work to investigate whether the ORC is effective for the hysteresis compensation during high-speed raster scanning of the piezo-actuated nanopositioning stages. This work provides an alternative approach to deal with the hysteresis nonlinearity, especially for the case of high input frequencies. The developed ORC strategy can be easily retrofitted to other piezo-actuated nanopositioning systems to improve the raster scanning performance by directly plugging it into the existing feedback control loop without changing the original controller.

In the rest of this paper, the hysteresis investigation and the ORC strategy design are presented in Section 2. In Section 3, the experimental setup and controller parameters design are presented. The effectiveness of the developed control approach is demonstrated by comparative experiments in Section 4, followed by the conclusion in Section 5.

2. Hysteresis investigation and ORC design

In this section, the effect of hysteresis nonlinearity on the nanopositioning system under triangular reference input is investigated first. Then, the ORC strategy is designed and its stability and robust stability conditions are both provided.

2.1. Hysteresis investigation

As analyzed in Section 1, the inherent hysteresis nonlinearity of the PSAs severely degrades the raster scanning performance of the nanopositioning stages, especially in the case of high-speed raster scanning. In this work, we attempt to investigate the hysteresis nonlinearity from a new perspective, which would make it possible to find an alternative control strategy to account for the hysteresis without constructing and inverting the complicated hysteresis model.

In general, the hysteresis nonlinearity can be represented as $w(t) = H[v](t)$, as shown in Fig. 1(a), where $w(t)$ is the hysteresis output that is usually unmeasurable, and $v(t)$ is the voltage input applied to the PSA. Following the derivation in [23,27], the system with hysteresis nonlinearity can be decomposed as a linear time-invariant plant $P(s)$ with a bounded input disturbance $d_h(t)$ resulting from the hysteresis, as shown in Fig. 1(b).

Remark 1. There are two assumptions when the hysteresis is treated as a disturbance $d_h(t)$. The first one is that the input–output relationship of piezo-actuated nanopositioning stages can be described by a cascade model consisting of a hysteresis operator $H[v](t)$ followed by a linear dynamics [18], as shown in Fig. 1(a). With this assumption, the hysteresis can be further decomposed as a disturbance $d_h(t)$. As a matter of fact, this assumption is widely adopted in the literature [8,9,18,26]. In particular, it is experimentally validated to be realistic in [18]. The second assumption is that the disturbance $d_h(t)$ is bounded. This assumption is also extensively utilized in the literature [11,12,27]. In addition, it can be found from Fig. 8 in this work that the hysteresis is bounded. Thus, the disturbance $d_h(t)$ must also be bounded and this assumption is realistic.

In our previous work [23], we have theoretically analyzed that, for a periodic reference input $v(t)$, the disturbance $d_h(t)$ resulting from the hysteresis is also periodic, i.e. $d_h(t+T) = d_h(t)$, where T is the period of the reference $v(t)$. This means, from the perspective of frequency domain, the $d_h(t)$ would affect the system at the fundamental frequency and the harmonics of the input signal.

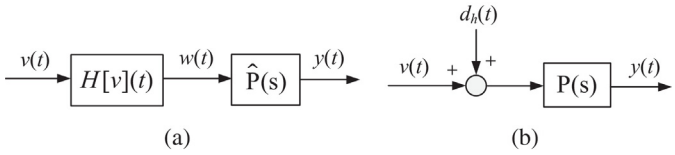

Fig. 1. Hysteresis investigation of the piezo-actuated nanopositioning stages. (a) Schematic of the nanopositioning system with hysteresis nonlinearity. (b) Schematic of the system with hysteresis decomposition.

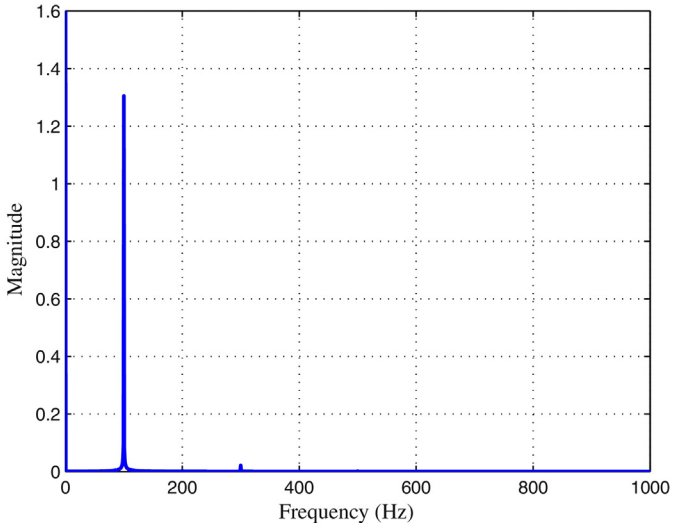

Fig. 2. Spectra of system output under sinusoidal reference input of $v(t) = 50 + 30\sin(200\pi t)$.

To further investigate the hysteresis effect in the frequency domain, new experiments are performed with a custom-built piezo-actuated nanopositioning stage using the sinusoidal reference inputs. More detailed introduction to this nanopositioning stage can be referred to [28] and more information about the experimental setup can be referred to the following Section 3.1. By analyzing the output of the piezo-actuated nanopositioning stage in the frequency domain, it is found that under sinusoidal reference input the spectra of the output mainly occur at the fundamental frequency and the third harmonic of the input signal. As an illustration, Fig. 2 shows the spectra of system output under sinusoidal signal input of $v(t) = 50 + 30\sin(200\pi t)$. As can be seen, the magnitudes of the output mainly occur at the frequencies of 100 Hz and 300 Hz and the magnitudes at other frequencies are negligible. There is no doubt that the 300-Hz component is caused by the hysteresis nonlinearity. Although the output at 100 Hz resulting from the hysteresis effect cannot be exactly determined, it can be deduced that the hysteresis nonlinearity mainly affects the system at the first two odd harmonics of the input frequency. During the raster scanning process of AFMs, the reference trajectory of piezo-actuated nanopositioning stages is triangular signal which can be represented in the Fourier series form with the odd harmonics of the fundamental frequency. Hence, it is intuitive to think whether the hysteresis-caused disturbance $d_h(t)$ under triangular reference input mainly affects the system at the odd harmonics of the fundamental frequency of the triangular input. To verify this thought, the system outputs $y(t)$ under triangular reference inputs $v(t)$ with different fundamental frequencies (50, 500, 1000, and 1562.5 Hz) are measured and analyzed. It should be noted that the triangular references used in this work are all constructed with the first seven odd harmonics (i.e. first, third, fifth, seventh, ninth, eleventh, and thirteenth harmonics). The input–output relationship in the time domain is shown in Fig. 8 in Section 4.1, where obvious hysteresis nonlinearity can be observed. In this section, the system output $y(t)$ is analyzed in the frequency domain and the spectra of $y(t)$ are shown in Fig. 3. As can be seen, with each triangular reference input, the magnitudes of the system output mainly occur at the first seven odd harmonics of the fundamental frequency of the input signal (the magnitudes at other frequencies are so small that can be ignored). This indicates that, with triangular reference input, the $d_h(t)$ mainly affects the piezo-actuated stage at the odd harmonics of the input signal. Hence, $d_h(t)$ can be treated as odd-harmonic periodic disturbance. It should be noted that the small magnitudes of eleventh and thirteenth harmonics of the system output under 1562.5-Hz triangular signal input (as can be observed from Fig. 3(d)) are due to the quick roll-off system characteristic after resonant frequency.

As the ORC strategy is well effective in mitigating the odd-harmonic periodic disturbances, it is developed in this work to deal with the hysteresis nonlinearity by suppressing the odd-harmonic disturbance $d_h(t)$ resulting from hysteresis. Thus, the modeling and inverting of complicated hysteresis nonlinearity are avoided. In

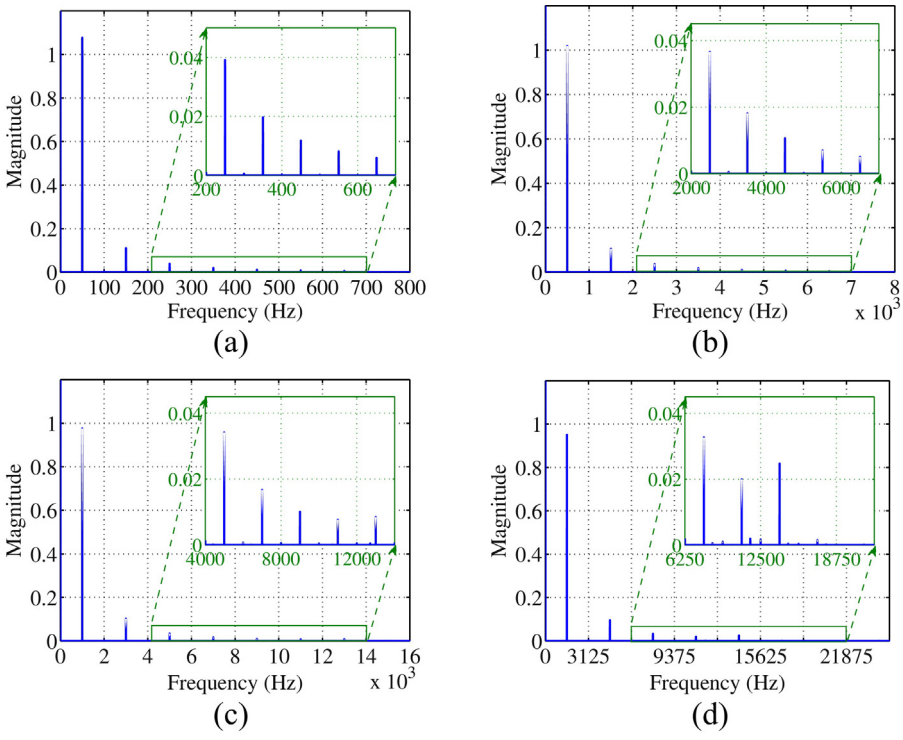

Fig. 3. Spectra of system output under triangular inputs at (a) 50 Hz; (b) 500 Hz; (c) 1000 Hz; (d) 1562.5 Hz.

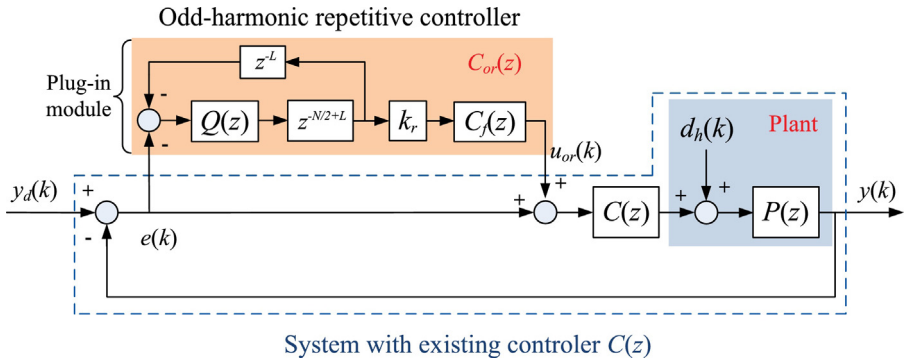

Fig. 4. The block diagram of system with the odd-harmonic repetitive control.

addition, as the triangular reference can be constructed using the odd harmonics of the fundamental frequency, the tracking errors caused by the linear dynamics effect are also odd-harmonic periodic signals according to the frequency response characteristics of linear systems. Hence, the ORC strategy can account for both disturbances/errors caused by hysteresis nonlinearity and linear dynamics during high-speed raster scanning.

2.2. ORC design

RC is an application of the internal model principle [29] for tracking periodic trajectories and rejecting periodic disturbances. The generally utilized RC is a control scheme for linear systems and the hysteresis nonlinearity of the PSAs restricts its implementation to nanopositioning stages. In this development, as the hysteresis nonlinearity is decomposed in Section 2.1, the nanopositioning stage can be deemed as a linear system with a bounded periodic disturbance. Hence, the RC strategy can be designed based on the linear system.

As analyzed in Section 2.1, during raster scanning process of AFMs, the disturbances/errors resulting from the hysteresis and linear dynamics mainly affect the nanopositioning system at odd harmonics of the input signal. Hence, the ORC strategy is developed in this work to deal with such odd-harmonic periodic disturbances/errors. The ORC strategy employs a signal generator $(-1/(z^{N/2}+1))$ into the feedback loop to provide high-gain control only at odd harmonics of the reference trajectory. Such signal generator needs $N/2$ memory cells, which is only a half of that CRC needs. Hence, it is beneficial for the real-time implementation. This is why the ORC rather than the CRC is adopted in this work to achieve high-speed raster scanning of the piezo-actuated nanopositioning stages with hysteresis nonlinearity. It should be noted that, although the ORC strategy has been demonstrated effective for power electronics systems [24,25], to the best knowledge of the authors, this work is the first attempt at introducing it for hysteresis compensation during raster scanning of piezo-actuated nanopositioning stages. Moreover, different from the minimum-phase power electronics systems as in [25,30], the typical piezo-actuated nanopositioning stages generally have non-minimum-phase zeros [31], which is due to the non-collocated actuators and sensors. Such non-minimum-phase characteristic limits the direct application of the ORC strategy in [25,30] which is tailored for minimum-phase systems. Hence, in this work, the ORC strategy is modified to make it suitable for the non-minimum-phase systems. Moreover, the stability and robust stability conditions for such ORC strategy are analyzed as well.

The control structure of the ORC strategy is shown in Fig. 4, where $y_d(k)$ is the desired reference, $y(k)$ is the actual output of the plant, $e(k)=y_d(k)-y(k)$ is the tracking error, $d_h(k)$ is the disturbance resulting from the hysteresis, $C(z)$ is an existing feedback controller for plant $P(z)$, $C_{or}(z)$ is the plug-in odd-harmonic repetitive controller, k_r is the repetitive control gain, $C_f(z)$ is a filter to ensure the closed-loop stability, $Q(z)$ is a low-pass filter to improve the robustness of the overall system, z^{-L} is the sum of the plant delay and controller delay, which results from the non-minimum-phase characteristic. The difference between the control structure in this work and that in [25,30] for minimum-phase systems lies in the terms of z^{-L} and $C_f(z)$.

It can be observed from Fig. 4 that the odd-harmonic repetitive controller $C_{or}(z)$ is a plug-in module, which is implemented by plugging it into the system with an existing controller $C(z)$. As the tracking error $e(k)$ is the only signal that the $C_{or}(z)$ directly used, in practical application $C_{or}(z)$ can be simply implemented by two steps: (i) capture the tracking error $e(k)$ which is generally available and utilize it as the input to the controller $C_{or}(z)$; (ii) apply the control output $u_{or}(k)$ of $C_{or}(z)$ as the input to the existing controller $C(z)$ together with the tracking error $e(k)$. It should be noted that the original controller $C(z)$ is kept unchanged when the $C_{or}(z)$ is plugged into the feedback loop prior to C(z), which makes the implementation of $C_{or}(z)$ easy. Also, $C(z)$ can be designed independently without consideration of $C_{or}(z)$. For $C(z)$, control approaches such as proportional-integral-derivative control [20] and H_∞ control [22] can be adopted. Without loss of generality, assume that the feedback controller $C(z)$ can keep the system asymptotically stable. Then, the complementary sensitivity function $H(z)$ of the closed-loop system with $C(z)$ (without $C_{or}(z)$) is expressed as

$$H(z)=\frac{C(z)P(z)}{1+C(z)P(z)}=z^{-d}\frac{B(z)}{A(z)}=z^{-d}\frac{B_s(z)B_u(z)}{A(z)} \tag{1}$$

where d represents the relative degree of $H(z)$, $B_s(z)$ includes all the stable zeros which are invertible, and $B_u(z)$ comprises all the unstable zeros that are not in $B_s(z)$.

Then, the ORC can be designed based on $H(z)$. The design method of the ORC is similar to that of CRC in [32]. The filter $C_f(z)$ is determined first. Different from the $C_f(z)$ for minimum-phase systems which can be derived by directly inverting $H(z)$ [25,30], the filter $C_f(z)$ here for non-minimum-phase systems is chosen as an approximate inversion of $H(z)$ on the basis of the zero-phase-error-tracking (ZPET) technique [33], i.e.

$$C_f(z)=z^{-(nc+nu)}\frac{A(z)B_u^f(z)}{B_s(z)b} \tag{2}$$

$$b\geq\max_{\omega\in[0,\ \pi/T_s]}|B_u(e^{j\omega T_s})|^2 \tag{3}$$

where $B_u^f(z)$ is derived by flipping the polynomial coefficients of $B_u(z)$, nu is the number of the zeros in $B_u(z)$ and nc is the additional delays added to keep $C_f(z)$ causal for real-time implementation. The choice of b in (3) is intended to keep the asymptotical stability of the ORC strategy. Obviously, $nc=O(A(z)B_u^f(z))-O(z^{nu}B_s(z))=nu$.

Then, the sum of the delay terms in $H(z)$ and $C_f(z)$, i.e. L, can be obtained as

$$L = d + nc \tag{4}$$

Generally, it is not possible in practice to establish a perfectly accurate model of $P(z)$, especially at high frequencies. Since the ORC also includes high-gain control in the high-frequency region, it may excite the unmodeled dynamics of the plant and induce instability during implementation. To improve the robustness of the system, a zero-phase low-pass filter $Q(z)$ is employed in the ORC control loop as follows

$$Q(z) = (a_1 z + a_2 + a_1 z^{-1})^i \tag{5}$$

where a_1 and a_2 satisfy $2a_1 + a_2 = 1$, and i is a positive integer. Although $Q(z)$ is a non-causal filter, its application can be ensured by the delay terms $z^{-N/2+L}$ in $C_{or}(z)$. It should be noted that since $Q(z)$ reduces the control gains of ORC in the high-frequency region to improve the robustness of the system, it would also deteriorate the tracking accuracy. Therefore, the tradeoff between the robustness and tracking accuracy should be made when selecting the parameters of $Q(z)$.

Finally, the odd-harmonic repetitive controller $C_{or}(z)$ can be derived as

$$C_{or}(z) = -\frac{k_r Q(z) z^{-N/2+L} C_f(z)}{1 + Q(z) z^{-N/2}} \tag{6}$$

2.3. Stability and robust stability

This subsection analyzes the stability and robust stability conditions of the ORC strategy which is applied to non-minimum-phase systems with the approximate inversion of H(z) on the basis of ZPET technique. The stability condition will provide guidance for the selection of the repetitive control gain k_r and the robust stability condition will impose a constraint on the design of all the controller parameters in $C_{or}(z)$, especially the design of the low-pass filter.

Theorem 1 (Stability). *Assume that the closed-loop system with feedback controller $C(z)$ is asymptotically stable, i.e. $1 + P(z)C(z) = 0$ has no roots outside the unit circle in the z-plane. Then, the closed-loop system with the ORC as shown in Fig. 4 is asymptotically stable as long as*

$$0 < k_r < 2 \tag{7}$$

Proof. See Appendix A. □

Theorem 2 (Robust stability). *Let the plant be perturbed as $\widetilde{P}(z) = P(z)(1 + \Delta_p(z))$, where $\Delta_p(z)$ is the model uncertainty. Assume that the feedback controller $C(z)$ and the ORC can stabilize $P(z)$. Then, a sufficient condition for the robust stability of the closed-loop system with the model uncertainty $\Delta_p(z)$ is given as*

$$|\Delta_p(z)|_{z=e^{j\omega T_s}} < \left| \frac{1 + (1 + C_{or}(z))C(z)P(z)}{(1 + C_{or}(z))C(z)P(z)} \right|_{z=e^{j\omega T_s}} \tag{8}$$

for $\omega \in [0, \pi/T_s]$.

Proof. See Appendix B. □

3. Application to nanopositioning stages

This section presents the implementation of the developed ORC strategy to nanopositioning stages. The experimental setup of the nanopositioning stage is established first. Then, the system model is identified and the controller parameters are designed.

3.1. Experimental setup

In this work, a piezo-actuated XY parallel-kinematic nanopositioning stage designed in our previous work [28] is adopted to validate the effectiveness of the developed ORC based control approach. The detailed description of the piezo-actuated nanopositioning stage can be referred to [28]. A dSPACE-DS1103 board equipped with the 16-bit analog to digital converters (ADCs) and 16-bit digital to analog converters (ADCs) is utilized to implement real-time control laws in the MATLAB/Simulink environment, which are then directly downloaded to the DS1103 control board via the ControlDesk interface for realtime applications. The DACs produce analog control input (0–10 V) and a high-voltage amplifier (HVA) with a fixed gain of 20 is used to provide excitation voltage (0–200 V) for the PSAs. Capacitive sensors (Probe 2823 and Gauging Module 8810 from MicroSense, range of $\pm\mu m$ with analog output of $\pm$10 V) are adopted to measure the displacements of the end-effector of the stage. The sensor output signals are captured by a signal conditioner (Gauging Module 8810) and simultaneously acquired by the ADCs for feedback control. In this work, the sampling frequency of the system is set to 50 kHz. The block diagram of the experimental setup is shown in Fig. 5.

Remark 2. The adopted custom-built piezo-actuated nanopositioning stage in this work is designed to be well decoupled, as experimentally validated in our previous work [28]. Therefore, when it is used for a raster-type scanning application in AFMs, the changing state of the linear axis (say X-axis) would affect little on the performance of the Y-axis and the two-axis motions can be treated independently. In this sense, the cross-couplings between two axes are not considered in the controller design and thus the developed ORC strategy can be directly implemented for the Y-axis. For the purpose of verifying the developed ORC based control

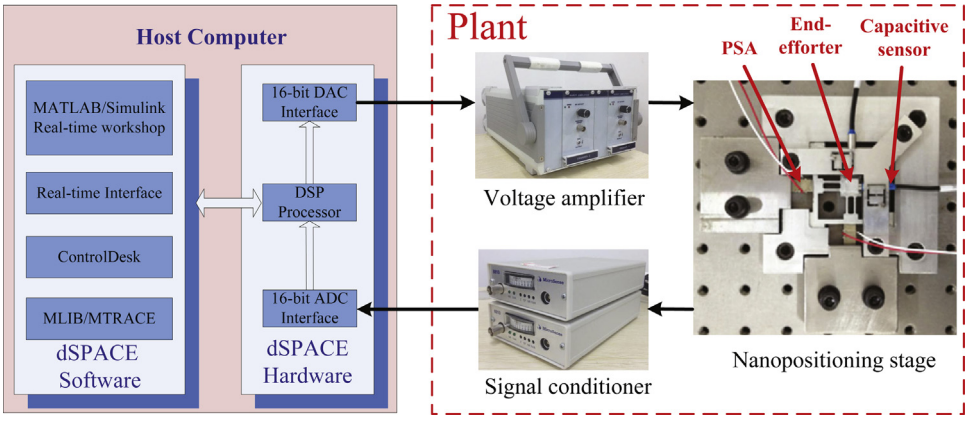

Fig. 5. The experimental setup.

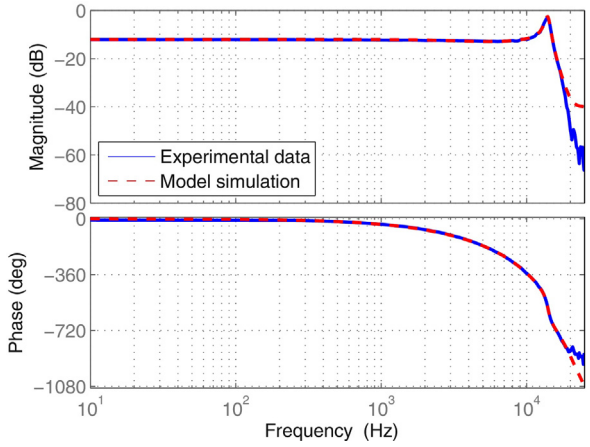

Fig. 6. Comparison of the measured frequency response and the simulated frequency response with the identified model. (For interpretation of the references to color in text near the reference citation, the reader is referred to the web version of this article.)

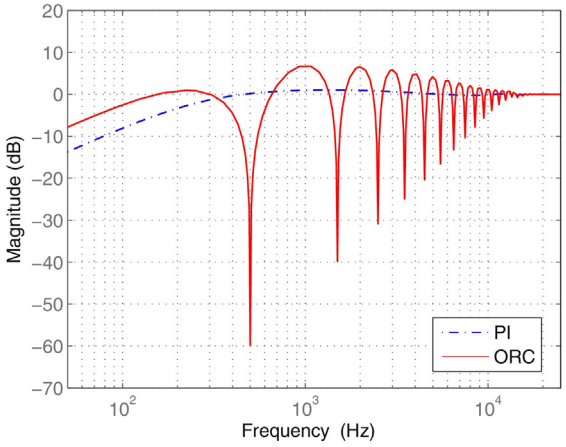

Fig. 7. Sensitivity plot of PI control and ORC strategy.

approach, only the treatment of *Y*-axis tracking control is presented in this work.

3.2. System model identification

As analyzed in Section 2.1, the nanopositioning system can be treated as a linear system with a bounded input disturbance. To identify the linear system, a band-limited white noise signal is used to excite the system. The dSPACE control system is utilized to simultaneously capture the excitation voltage and the corresponding measured displacement. Then, a spectral analysis is performed to obtain the frequency response, as shown in Fig. 6, where the blue solid line is the experimental result. It can be observed from the figure that the measured resonant frequency of the *Y*-axis is 13.9 kHz. Based on the experimental data, a sixth-order plant model $P(z)$ is identified with the System Identification Toolbox of MATLAB, which is expressed as

$$P(z) = \frac{-5.662 \times 10^{-5} z^5 + 0.0005 z^4 + 0.0038 z^3 + 0.0509 z^2 + 0.1149 z + 0.1032}{z^6 - 0.4354 z^5 + 1.013 z^4 - 0.6771 z^3 + 0.3096 z^2 - 0.1197 z} \tag{9}$$

The red dashed line in Fig. 6 shows the frequency response of the identified model. It can be observed that the frequency response of the identified model accurately matches the frequency response of the measured data in a wide frequency range.

3.3. Controller parameters design

Since proportional-integral (PI) controller is the most popular control technique used in the commercial AFMs [21], it is chosen as the existing feedback controller $C(z)$ in this work. The transfer function of a discrete PI controller can be expressed as $C(z) = K_p + K_i \frac{T_s}{z-1}$, where K_p and K_i are the proportional and integral gains, respectively, and T_s is the sampling time of the system. The control gains of PI controller are initially selected by the simulation in MATLAB/Simulink, and then tuned by the trial and error method as $K_p = 0.1$ and $K_i = 6000$. Based on the dynamic model $P(z)$ and feedback controller $C(z)$, the ORC can be designed with (1)–(6). In this work, b is chosen as $b = (|b_0| + |b_1| + \cdots |b_{nu}|)^2$ [32], which satisfies (3). The low-pass filter (5) is chosen as $Q(z) = 0.25z + 0.5 + 0.25z^{-1}$ to reduce the control gains of ORC at high frequencies. The repetitive control gain k_r is chosen by simulation studies as $k_r = 1$. It is noted that the selected parameters satisfy the stability and robust stability conditions of (7) and (8).

Before experimental evaluation, the controller performance of the PI control and developed ORC strategy is theoretically analyzed. The magnitude of the sensitivity function of the PI control is plotted in Fig. 7. As can be seen from the figure, due to the limited control bandwidth, the PI control cannot account for the tracking errors caused by the linear dynamics at the frequencies above 500 Hz. The magnitude of the sensitivity function of the ORC strategy in Eq. (A.1) is also plotted in Fig. 7 with $N = 100$ as an illustrative example, which corresponds to the input frequency of 500 Hz. It can be seen from the figure that, with the ORC strategy, deep notches occur at the odd harmonics of 500 Hz. This indicates that the tracking errors caused by the linear dynamics effect, which are at these odd harmonics in the raster scanning application, would be significantly reduced. It should be noted that the bode response of the transfer function from the input disturbance $d_h(k)$ to the tracking error $e(k)$ shows the similar shape with $S(z)$, i.e. there are also deep notches at the odd harmonics of the fundamental input frequency. This is why the ORC strategy can deal with the disturbance resulting from the hysteresis nonlinearity. As the ORC strategy can account for both disturbances/errors caused by the hysteresis nonlinearity and linear dynamics, the ORC is capable of improving the tracking speed and accuracy as compared with the PI control during raster scanning.

Additionally, it can be observed from the Fig. 7 that the magnitude of these notches gradually decreases as the frequency increases, which yields the reduction of control capacity of the ORC in the high-frequency region. Such effect is due to the introduction of the low-pass filter $Q(z)$ in the control loop. Generally, higher cut-off frequency of $Q(z)$ tends to result in better tracking accuracy of ORC. However, this also reduces the robustness of the controller and may incur instability. Hence, the cut-off frequency of $Q(z)$ should be carefully determined based on the desired control performance.

Remark 3. In this work, the coefficients of $Q(z)$ are selected with trial and error method in simulation, which is a commonly used method in the literature for determining the parameters of the low-pass filter in repetitive controllers [21,22,26]. In fact, when the maximum allowable tracking errors at specific frequencies (the odd harmonics of the fundamental frequency) are predefined, the parameters of $Q(z)$ may be determined through an optimization procedure with the following possible constraints: (i) the value of sensitivity function $S(z)$ in (A.1) at each specific frequency should ensure that the tracking error at this frequency does not exceed the maximum allowable value; (ii) the robust stability condition (8) should be satisfied; and (iii) the coefficients of $Q(z)$ should meet that $2a_1 + a_2 = 1$.

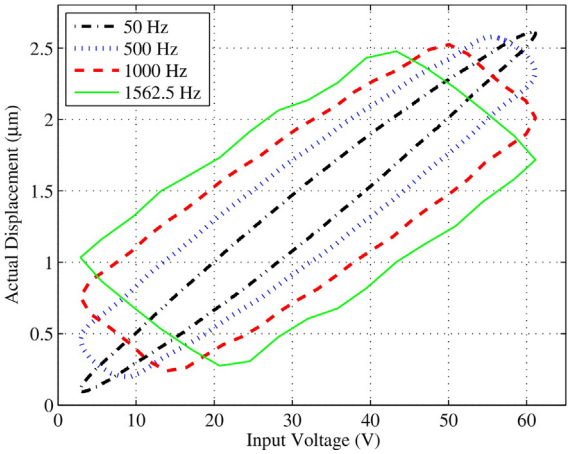

Fig. 8. Relation between the measured displacement and the input voltage in the open-loop case under triangular reference inputs with different fundamental frequencies.

4. Experimental studies

In this section, the performance of the developed ORC strategy is evaluated with various experiments.

4.1. Open-loop test

Before implementation of the ORC strategy, open-loop test of the piezo-actuated nanopositioning stage is first performed to measure the hysteresis nonlinearity. Fig. 8 shows the relations between the measured displacement and the input voltage under triangular reference inputs with various fundamental frequencies. As can be seen, the piezo-actuated nanopositioning stage exhibits obvious hysteresis nonlinearity in the open-loop strategy. Moreover, it can be observed that the hysteresis nonlinearity becomes severer as the input frequency increases. In this work, to quantify the hysteresis effect, the hysteresis percentage is utilized as an index which is defined as the maximum hysteresis height with respect to the maximum displacement range. The hysteresis percentages in the open-loop case for different input frequencies are listed in the second column in Table 2. It can be found that the hysteresis percentage becomes larger with the increase of the input frequency and it is up to 72.86% for 1562.5-Hz triangular reference input.

It can be also seen from Fig. 8 that, at the input frequency of 1562.5 Hz, the hysteresis loop becomes more complex and corrugations appear. This is due to the coupling effect of the hysteresis nonlinearity and linear dynamics effect, as the ninth harmonic component of the input signal is around the resonant frequency (13.9 kHz) of the nanopositioning stage and excites the resonance. Such excitation can be obviously found from Fig. 3(d), as the ninth harmonic component is amplified and it is even larger than the seventh harmonic component. It should be noted that the coupling effect between the hysteresis nonlinearity and the linear dynamics makes it more challenging to develop effective controllers for high-speed raster scanning of piezo-actuated nanopositioning stages. Generally, it is difficult to construct a hysteresis model to accurately describe such severe hysteresis nonlinearity which is coupled with the linear dynamics, not to mention the compensation of it. Hence, development of new methods to deal with the hysteresis nonlinearity especially at high input frequencies is necessary. This is our motivation to develop the ORC strategy in this work, which is aimed at providing an approach to mitigate the hysteresis nonlinearity during high-speed raster scanning. Its effectiveness on hysteresis compensation will be validated in the following subsections.

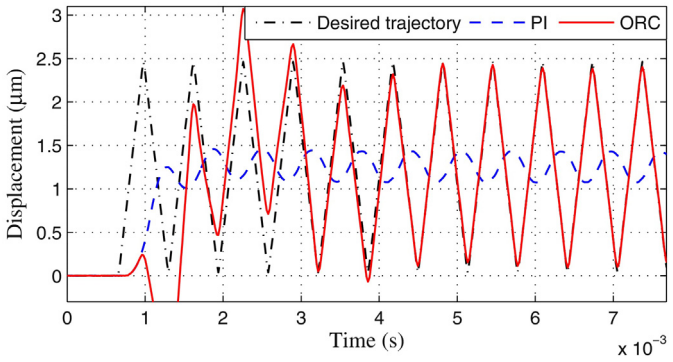

Fig. 9. Raster scanning results with the PI control and ORC under the 1562.5-Hz triangular trajectory.

4.2. Raster scanning test

The raster scanning test is conducted on the piezo-actuated nanopositioning stage under triangular trajectories with various input frequencies. As the PI control is chosen as the existing feedback controller $C(z)$ in this work, comparisons are made between the developed ORC strategy and PI control to verify effectiveness of the ORC on the tracking performance improvement. It should be noted that the parameters of the PI controller are the same with those of the PI controller in the ORC strategy.

As an illustration, the raster scanning results with PI control and ORC strategy under 1562.5-Hz triangular trajectory are shown in Fig. 9. It is obvious that the tracking performance with ORC is significantly better than that with PI control. This is further validated by Fig. 10, which shows the comparisons of the tracking errors with PI control and ORC under triangular trajectories with different fundamental frequencies. It can be seen from Fig. 10 that with the increase of the input frequency, the tracking performance of the PI control is severely degraded. In contrast, the developed ORC strategy presents a more robust performance at different input frequencies. For a quantitative comparison, Table 1 summarizes the steady-state maximum tracking error (e_m (%)) and root-mean-square tracking error (e_{rms} (%)) of PI control and ORC under triangular reference with input frequencies of 50, 500, 1000, and 1562.5 Hz. It can be seen that the e_m and e_{rms} with PI control can be up to 55.40% and 33.64%, respectively, under 1562.5-Hz reference input, which indicates that the PI control loses its effectiveness for high-speed raster scanning. By contrast, the steady-state tracking errors e_m and e_{rms} with ORC are 3.16% and 0.85%, respectively, which are much lower than those with PI control. Therefore, it is demonstrated that the developed ORC strategy can effectively improve the tracking performance of the nanopositioning stage in the raster scanning applications. In addition, it is worthy of mentioning that the developed ORC strategy can be easily retrofitted to other piezo-actuated nanopositioning systems to enhance the raster scanning performance by directly plugging it into the existing feedback control loop without changing the original controller.

Table 1
Comparison of steady-state tracking errors of the PI control and ORC under triangular trajectories with various fundamental frequencies.

Frequency (Hz)	PI		ORC	
	e_m (%)	e_{rms} (%)	e_m (%)	e_{rms} (%)
50	6.33	4.89	0.30	0.062
500	47.18	31.48	0.60	0.24
1000	55.39	34.16	1.58	0.49
1562.5	55.40	33.64	3.16	0.85

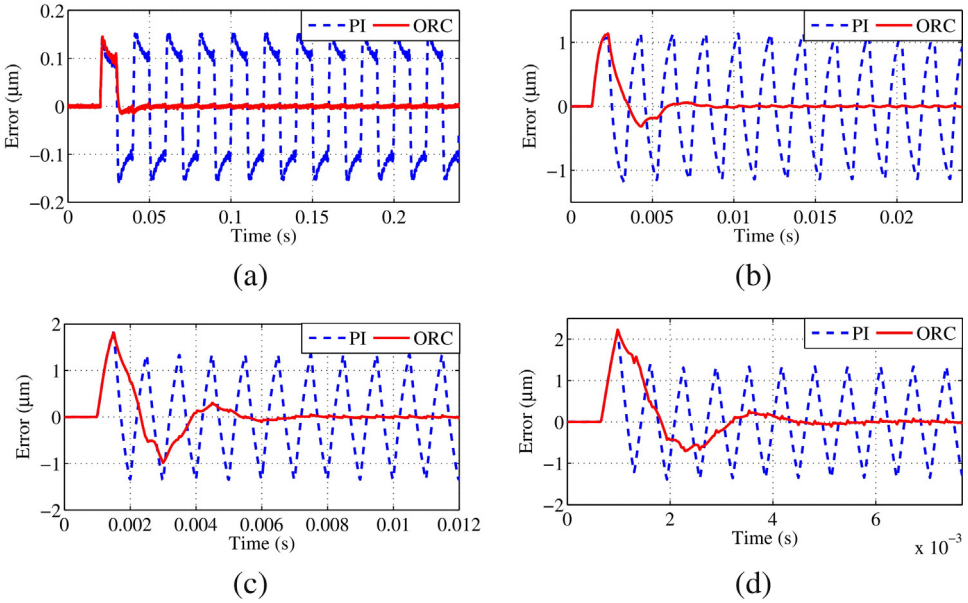

Fig. 10. Comparison of tracking errors of the PI control and ORC under triangular trajectories with fundamental frequencies of (a) 50 Hz, (b) 500 Hz, (c) 1000 Hz, and (d) 1562.5 Hz.

4.3. Hysteresis compensation test

To evaluate the performance of the developed control strategies on hysteresis compensation, Fig. 11 shows the relations between the actual and desired displacements with PI control and ORC in the raster scanning tests under different input frequencies, respectively. As can be observed, the experimental results with PI control still exhibit obvious nonlinear effect. By contrast, the ORC strategy effectively suppresses the hysteresis nonlinearity at these different input frequencies and the input–output relation of the system is almost linear. The hysteresis compensation result with ORC strategy is also tabulated in the fourth column of Table 2. As can be seen, the hysteresis percentage with ORC under 1562.5-Hz triangular reference input is only 1.44%, which is reduced by 98.02% as compared to that in the open-loop case. The results demonstrate the effectiveness of the developed ORC strategy on hysteresis compensation during high-speed raster scanning.

4.4. Accounting for linear dynamics test

Besides hysteresis compensation, another benefit of the ORC strategy is that it can also account for the tracking errors caused

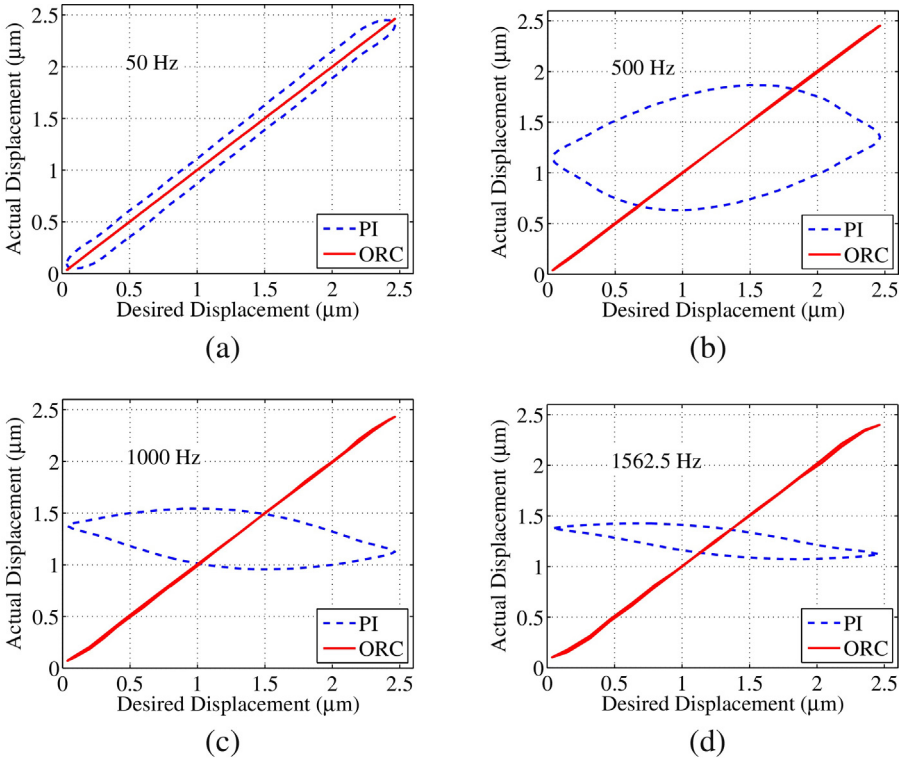

Fig. 11. Hysteresis compensation results using PI control and ORC under triangular references with input frequencies of (a) 50 Hz, (b) 500 Hz, (c) 1000 Hz, and (d) 1562.5 Hz.

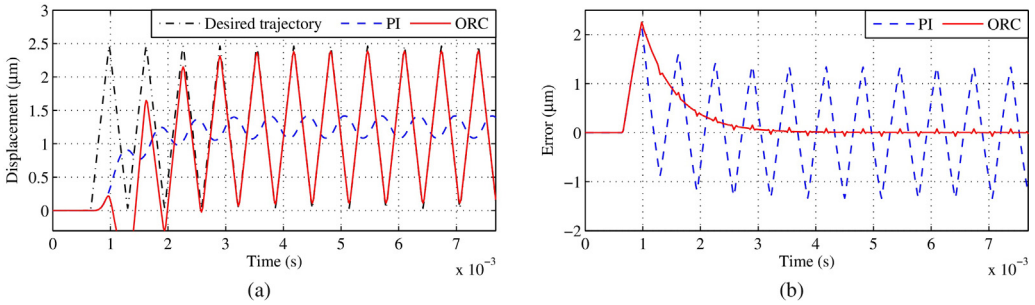

Fig. 12. The simulation results of raster scanning with the PI control and ORC strategy under the 1562.5-Hz triangular trajectory. (a) Trajectory tracking; (b) Tracking error.

Table 2
Hysteresis effect compensation with different control strategies.

Frequency (Hz)	Hysteresis percentage (%)		
	Open loop	PI	ORC
50	15.71	10.40	0.22
500	33.72	–	0.87
1000	51.82	–	1.03
1562.5	72.86	–	1.44

by the linear dynamics effect, which has been theoretically analyzed in Section 3.3. As the experimental results include both the influences of hysteresis and linear dynamics effects, it is hard to distinguish the performance of the controllers to account for linear dynamics. Hence, this performance is investigated in simulation using the identified plant model (9), where the tracking errors are only caused by the linear dynamics. As an illustration, the simulation results of raster scanning with the PI control and the ORC strategy under 1562.5-Hz triangular trajectory are shown in Fig. 12. As can be seen, the PI control results in large tracking errors, which is due to its limited control bandwidth that cannot deal with the linear dynamics in the high frequencies. By contrast, the ORC strategy significantly improves the tracking performance of PI control, which validates its performance to account for the linear dynamics.

5. Conclusion

In this paper, an ORC strategy is developed for high-speed raster scanning of piezo-actuated nanopositioning stages with hysteresis nonlinearity. Several distinctive features of this paper are summarized as follows: (1) it is experimentally found that, with triangular reference input, the hysteresis nonlinearity mainly affects the system at the odd harmonics of the input signal; (2) an ORC strategy which is suitable for non-minimum-phase systems is proposed to deal with both the hysteresis nonlinearity and linear dynamics, with the hysteresis nonlinearity treated as odd-harmonic periodic disturbance; (3) real-time experiments on a custom-built piezo-actuated stage are performed to demonstrate the feasibility and effectiveness of the developed ORC strategy for high-speed raster scanning, especially for the hysteresis compensation; (4) the developed ORC strategy can be easily retrofitted to other piezo-actuated nanopositioning systems to improve the raster scanning performance by plugging it into the existing feedback control loop without changing the original controller.

Acknowledgements

This work was supported by the National Natural Science Foundation of China under Grant No. 51405293, the Science and Technology Commission of Shanghai Municipality under Grant No. 15550722300, and the Specialized Research Fund for the Doctoral Programme of Higher Education under Grant No. 20130073110037.

Appendix A. Proof of Theorem 1

Proof. The sensitivity function $S(z)$ of the whole system can be derived as follows (for the sake of brevity, the z-domain index z is omitted here)

$$S = \frac{1}{1+(1+C_{or})PC} = \frac{1+Qz^{-N/2}}{(1+PC)(1+Qz^{-N/2}(1-k_r z^L C_f H))} \tag{A.1}$$

Then, it can be obtained that the characteristic polynomial of the closed-loop system is

$$D(z) = (1+P(z)C(z))(1+Q(z)z^{-N/2}(1-k_r z^L C_f(z)H(z))) \tag{A.2}$$

Since $(1+P(z)C(z))$ is stable by the assumption, the stability of the system depends on the second term on the right-hand side in (A.2). In view of small-gain theorem [34], $(1+Q(z)z^{-N/2}(1-k_r z^L C_f(z)H(z)))$ is stable if the following condition is satisfied:

$$|Q(z)z^{-N/2}(1-k_r z^L C_f(z)H(z))|_{z=e^{j\omega T_s}} < 1 \tag{A.3}$$

with $\omega \in [0, \pi/T_s]$. It can be easily derived from (1), (2) and (4) that $z^L C_f(z)H(z) = B_u(z)B_u(z^{-1})/b$, where $B_u(z^{-1})$ is obtained from $B_u(z)$ by replacing z with z^{-1}. As $|Q(z)|_{z=e^{j\omega T_s}} < 1$ and $|z^{-N/2}|_{z=e^{j\omega T_s}} = 1$, it can be deduced that (A.3) is met once the following condition holds:

$$\left|1 - \frac{k_r B_u(z)B_u(z^{-1})}{b}\right|_{z=e^{j\omega T_s}} < 1 \tag{A.4}$$

with $\omega \in [0, \pi/T_s]$. Since $B_u(z)B_u(z^{-1})_{z=e^{j\omega T_s}} = |B_u(e^{j\omega T_s})|^2$, taking into account (3) and (A.4), it allows the derivation that the closed-loop system with the ORC as shown in Fig. 4 is asymptotically stable as long as

$$0 < k_r < 2 \tag{A.5}$$

□

Appendix B. Proof of Theorem 2

Proof. From (A.1), the sensitivity function of the closed-loop system with plant $\tilde{P}(z)$ can be expressed as

$$\tilde{S}(z) = \frac{1}{1+(1+C_{or}(z))C(z)P(z)(1+\Delta_p(z))} \tag{B.1}$$

Then, the characteristic polynomial of the closed-loop system with modeling uncertainty can be derived as

$$\begin{aligned}\tilde{D} &= 1+(1+C_{or})CP(1+\Delta_p) \\ &= (1+(1+C_{or})CP) \times \left(1 + \frac{(1+C_{or})C_p}{1+(1+C_{or})CP}\Delta_p\right)\end{aligned} \tag{B.2}$$

where $(1+(1+C_{or})CP)$ is stable by assumptions. Hence, the robust stability of the closed-loop system depends on the stability of the second term on right-hand side in (B.1). By applying the small-gain theorem [34], the stability condition for the second term of (B.1) is derived as

$$\left|\frac{(1+C_{or})C_p}{1+(1+C_{or})CP}\Delta_p\right| \le \left|\frac{(1+C_{or})C_p}{1+(1+C_{or})CP}\right||\Delta_p| < 1 \qquad \text{(B.3)}$$

Then, the robust stability condition (8) of the closed-loop system can be easily obtained from (B.3). □

References

[1] G. Schitter, P.J. Thurner, P.K. Hansma, Design and input-shaping control of a novel scanner for high-speed atomic force microscopy, Mechatronics 18 (5) (2008) 282–288.
[2] Y.K. Yong, S.O.R. Moheimani, B.J. Kenton, K.K. Leang, Invited review article: high-speed flexure-guided nanopositioning: mechanical design and control issues, Rev. Sci. Instrum. 83 (12) (2012) 121101.
[3] T. Ando, T. Uchihashi, T. Fukuma, High-speed atomic force microscopy for nano-visualization of dynamic biomolecular processes, Prog. Surf. Sci. 83 (7–9) (2008) 337–437.
[4] I. Casuso, J. Khao, M. Chami, P. Paul-Gilloteaux, M. Husain, J.P. Duneau, H. Stahlberg, J.N. Sturgis, S. Scheuring, Characterization of the motion of membrane proteins using high-speed atomic force microscopy, Nat. Nanotechnol. 7 (8) (2012) 525–529.
[5] Y. Tian, B. Shirinzadeh, D. Zhang, A flexure-based mechanism and control methodology for ultra-precision turning operation, Precis. Eng. 33 (2) (2009) 160–166.
[6] G.Y. Gu, L.M. Zhu, C.Y. Su, H. Ding, Modeling and control of piezo-actuated nanopositioning stages: a survey, IEEE Trans. Autom. Sci. Eng. 31 (2016) 3–33, 2.
[7] A.J. Fleming, S.O.R. Moheimani, A grounded-load charge amplifier for reducing hysteresis in piezoelectric tube scanners, Rev. Sci. Instrum. 76 (7) (2005) 073707.
[8] G.Y. Gu, L.M. Zhu, Motion control of piezoceramic actuators with creep, hysteresis and vibration compensation, Sens. Actuators A: Phys. 197 (2013) 76–87.
[9] Z. Guo, Y. Tian, X. Liu, B. Shirinzadeh, F. Wang, D. Zhang, An inverse Prandtl–Ishlinskii model based decoupling control methodology for a 3-DOF flexure-based mechanism, Sens. Actuators A: Phys. 230 (2015) 52–62.
[10] Z. Li, C.Y. Su, T.Y. Chai, Compensation of hysteresis nonlinearity in magnetostrictive actuators with inverse multiplicative structure for preisach model, IEEE Trans. Autom. Sci. Eng. 11 (2) (2014) 613–619.
[11] Q.S. Xu, Digital sliding-mode control of piezoelectric micropositioning system based on input–output model, IEEE Trans. Ind. Electron. 61 (10) (2014) 5517–5526.
[12] H.C. Liaw, B. Shirinzadeh, J. Smith, Enhanced sliding mode motion tracking control of piezoelectric actuators, Sens. Actuators A: Phys. 138 (1) (2007) 194–202.
[13] H. Habibullah, H.R. Pota, I.R. Petersen, M.S. Rana, Tracking of triangular reference signals using LQG controllers for lateral positioning of an AFM scanner stage, IEEE Trans. Mechatron. 19 (4) (2014) 1105–1114.
[14] J.M. Cruz-Hernández, V. Hayward, Phase control approach to hysteresis reduction, IEEE Trans. Control Syst. Technol. 9 (1) (2001) 17–26.
[15] E. Asua, V. Etxebarria, A. Garcia-Arribas, Neural network-based micropositioning control of smart shape memory alloy actuators, Eng. Appl. Artif. Intel. 21 (5) (2008) 796–804.
[16] X. Zhang, Y. Tan, A hybrid model for rate-dependent hysteresis in piezoelectric actuators, Sens. Actuators A: Phys. 157 (1) (2010) 54–60.
[17] W. Li, X. Chen, Compensation of hysteresis in piezoelectric actuators without dynamics modeling, Sens. Actuators A: Phys. 199 (17) (2013) 89–97.
[18] Y. Wu, Q.Z. Zou, Iterative control approach to compensate for both the hysteresis and the dynamics effects of piezo actuators, IEEE Trans. Control Syst. Technol. 15 (5) (2007) 936–944.
[19] Q.S. Xu, Y.M. Li, Dahl model-based hysteresis compensation and precise positioning control of an XY parallel micromanipulator with piezoelectric actuation, ASME J. Dyn. Syst. Meas. Control 132 (4) (2010) 041011.
[20] C.Y. Lin, P.Y. Chen, Precision tracking control of a biaxial piezo stage using repetitive control and double-feedforward compensation, Mechatronics 21 (1) (2011) 239–249.
[21] U. Aridogan, Y.F. Shan, K.K. Leang, Design and analysis of discrete-time repetitive control for scanning probe microscopes, ASME J. Dyn. Syst. Meas. Control 131 (6) (2009) 061103.
[22] Y.M. Li, Q.S. Xu, Design and robust repetitive control of a new parallel-kinematic XY piezostage for micro/nanomanipulation, IEEE/ASME Trans. Mechatron. 17 (6) (2012) 1120–1132.
[23] C.X. Li, G.Y. Gu, M.J. Yang, L.M. Zhu, High-speed tracking of a nanopositioning stage using modified repetitive control, IEEE Trans. Autom. Sci. Eng. (2015) 1–11, http://dx.doi.org/10.1109/TASE.2015.2428437.
[24] R. Costa-Castelló, R. Griñó, E. Fossas, Odd-harmonic digital repetitive control of a single-phase current active filter, IEEE Trans. Power Electron. 19 (4) (2004) 1060–1068.
[25] K.L. Zhou, K.S. Low, D.W. Wang, F.L. Luo, B. Zhang, Y.G. Wang, Zero-phase odd-harmonic repetitive controller for a single-phase PWM inverter, IEEE Trans. Power Electron. 21 (1) (2006) 193–201.
[26] Y.F. Shan, K.K. Leang, Dual-stage repetitive control with Prandtl–Ishlinskii hysteresis inversion for piezo-based nanopositioning, Mechatronics 22 (3) (2012) 271–281.
[27] C.Y. Su, Y. Stepanenko, J. Svoboda, T.P. Leung, Robust adaptive control of a class of nonlinear systems with unknown backlash-like hysteresis, IEEE Trans. Autom. Control 45 (12) (2000) 2232–2247.
[28] C.X. Li, G.Y. Gu, M.J. Yang, L.M. Zhu, Design, analysis and testing of a parallel-kinematic high-bandwidth XY nanopositioning stage, Rev Sci. Instrum. 84 (12) (2013) 125111.
[29] B.A. Francis, W.M. Wonham, The internal model principle of control theory, Automatica 12 (5) (1976) 457–465.
[30] R. Griñó, R. Costa-Castelló, Digital repetitive plug-in controller for odd-harmonic periodic references and disturbances, Automatica 41 (2005) 153–157.
[31] C. Lee, S.M. Salapaka, Robust broadband nanopositioning: fundamental trade-offs, analysis, and design in a two-degree-of-freedom control framework, Nanotechnology 20 (2009) 035501.
[32] M. Tomizuka, T.C. Tsao, K.K. Chew, Analysis and synthesis of discrete-time repetitive controllers, ASME J. Dyn. Syst. Meas. Control 111 (3) (1989) 353–358.
[33] M. Tomizuka, Zero phase error tracking algorithm for digital control, ASME J. Dyn. Syst. Meas. Control 109 (1) (1987) 65–68.
[34] C.A. Desoer, M. Vidyasagar, Feedback Systems: Input–output Properties, Academic, New York, 1975.

Biographies

Chun-Xia Li received the B.E. degree (with honors) in mechanical engineering from Shanghai Jiao Tong University, Shanghai, China, in 2011, where she is currently working toward the Ph.D. degree in mechanical engineering. Her research interests include compliant mechanisms, design and control of high-bandwidth nanopositioning stages. She was a recipient of the National Scholarship for Excellent Master Student granted by the Ministry of Education of China in 2012.

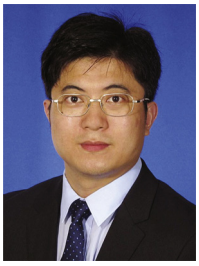

Guo-Ying Gu received the B.E. degree (with honors) in electronic science and technology, and the Ph.D. degree (with honors) in mechatronic engineering from Shanghai Jiao Tong University, Shanghai, China, in 2006 and 2012, respectively. He was a Visiting Scholar at Concordia University, Montreal, QC, Canada, and the National University of Singapore, Singapore. Supported by the Alexander von Humboldt Foundation, he was as a Humboldt Fellow at the University of Oldenburg, Oldenburg, Germany. Since October 2012, he has worked at Shanghai Jiao Tong University, where he is currently appointed as an Associate Professor with the School of Mechanical Engineering. His research interests include soft/continuum robots, smart material actuated devices and unmanned aerial vehicles. He has authored or co-authored over 40 publications in journals, book chapters and conference proceedings. He is a member of the American Society of Mechanical Engineers. Currently he serves as an Associate Editor of the International Journal of Advanced Robotic Systems. He has also served for several international conferences as Associate Editor or a program committee member.

Li-Min Zhu received the B.E. degree (with honors) and Ph.D. degree in mechanical engineering from Southeast University, Nanjing, China, in 1994 and 1999, respectively. From November 1999 to January 2002, he was a Postdoctoral Fellow with Huazhong University of Science and Technology, Wuhan, China. Since March 2002, he has been with Shanghai Jiao Tong University, Shanghai, China, where he is currently a "Cheung Kong" Chair Professor and the Vice Director of the State Key Laboratory of Mechanical System and Vibration. He has authored and coauthored one monograph and more than 190 peer reviewed papers, including 119 on international journals. His research interests include fixturing, CNC machining, and 3-D measurement of complex shaped parts and control, sensing, and instrumentation for micro/nano manufacturing. He was the recipient of National Distinguished Youth Scientific Fund of China in 2013. Now he serves as the Associate Editor of the IEEE Transactions on Automation Science and Engineering, and the Editorial Board Member of Proceedings of the IMechE, Part B: Journal of Engineering Manufacture.

Chun-Yi Su received his Ph.D. degree in control engineering from the South China University of Technology in 1990. After a seven-year stint with the University of Victoria, he joined Concordia University in 1998, where he is currently a Professor of Mechanical and Industrial Engineering and holds the Concordia Research Chair in Control. He has also held several short-time visiting positions including a Chang Jiang Chair Professorship by China's Ministry of Education and JSPS Invitation Fellowship from Japan. His research covers control theory and its applications to various mechanical systems, with a recent focus on control of systems involving hysteresis nonlinearities. He has authored or co-authored over 300 publications in journals, book chapters and conference proceedings. He has served as an Associate Editor of the IEEE Transactions on Automatic Control and the IEEE Transactions on Control Systems Technology. He has been on the Editorial Board of 18 journals, including the IFACs Control Engineering Practice and Mechatronics. He served for many conferences as an organizing committee member, including the General Co-Chair of the IEEE International Conference on Mechatronics and Automation in 2012 and the Program Chair of the IEEE Conference on Control Applications in 2007.